

This document is confidential and is proprietary to the American Chemical Society and its authors. Do not copy or disclose without written permission. If you have received this item in error, notify the sender and delete all copies.

Improving PM_{2.5} Forecasts in China Using an Initial Error Transport Model

Journal:	<i>Environmental Science & Technology</i>
Manuscript ID	es-2020-01680z.R1
Manuscript Type:	Article
Date Submitted by the Author:	06-Jul-2020
Complete List of Authors:	<p>Wu, Huangjian; Peking University, Guanghua School of Management and Center for Statistical Science</p> <p>Zheng, Xiaogu; Institute of Atmospheric Physics Chinese Academy of Sciences, CAS-TWAS Center of Excellence for Climate and Environment Sciences</p> <p>Zhu, Jiang; Institute of Atmospheric Physics Chinese Academy of Sciences, CAS-TWAS Center of Excellence for Climate and Environment Sciences (ICCES); University of the Chinese Academy of Sciences</p> <p>Lin, Wei; Peking University, School of Mathematical Sciences and Center for Statistical Science</p> <p>Zheng, Haitao; Anhui Institute of Optics and Fine Mechanics, Key Laboratory of Environmental Optics and Technology</p> <p>Chen, Xueshun; Institute of Atmospheric Physics Chinese Academy of Sciences, State Key Laboratory of Atmospheric Boundary Layer Physics and Atmospheric Chemistry; Institute of Urban Environment Chinese Academy of Sciences, Center for Excellence in Regional Atmospheric Environment</p> <p>Wang, Wei; China National Environmental Monitoring Center</p> <p>Wang, Zifa; Institute of Atmospheric Physics Chinese Academy of Sciences, State Key Laboratory of Atmospheric Boundary Layer Physics and Atmospheric Chemistry; University of the Chinese Academy of Sciences; Institute of Urban Environment Chinese Academy of Sciences, Center for Excellence in Regional Atmospheric Environment</p> <p>Chen, SongXi; Peking University, Guanghua School of Management and Center for Statistical Science</p>

SCHOLARONE™
Manuscripts

1 Improving PM_{2.5} Forecasts in China Using an Initial 2 Error Transport Model

3 *Huangjian Wu,^{*,†} Xiaogu Zheng,[‡] Jiang Zhu,^{‡,§} Wei Lin,^{*,‡} Haitao Zheng,[‡] Xueshun Chen,^{#,Δ} Wei
4 Wang,[°] Zifa Wang,^{#,§,Δ} and Song Xi Chen[†]*

5 [†]Guanghua School of Management and Center for Statistical Science, Peking University, Beijing
6 100871, China

7 [‡]CAS-TWAS Center of Excellence for Climate and Environment Sciences, Institute of
8 Atmospheric Physics, Chinese Academy of Sciences, Beijing 100029, China

9 [§]University of Chinese Academy of Sciences, Beijing 100049, China

10 [‡]School of Mathematical Sciences and Center for Statistical Science, Peking University, Beijing
11 100871, China

12 [‡]Key Laboratory of Environmental Optics and Technology, Anhui Institute of Optics and Fine
13 Mechanics, Chinese Academy of Sciences, Hefei, Anhui 230031, China

14 [#]State Key Laboratory of Atmospheric Boundary Layer Physics and Atmospheric Chemistry,
15 Institute of Atmospheric Physics, Chinese Academy of Sciences, Beijing 100029, China

16 ^ΔCenter for Excellence in Regional Atmospheric Environment, Institute of Urban Environment,
17 Chinese Academy of Sciences, Xiamen, Fujian 361021, China

18 [°]China National Environmental Monitoring Center, Beijing 100012, China

19

20 ABSTRACT

21 The efforts of using data assimilation to improve $\text{PM}_{2.5}$ forecasts have been hindered by the limited
22 number of species and incomplete vertical coverage in the observations. The common practice of
23 initializing a chemical transport model (CTM) with assimilated initial conditions (ICs) may lead
24 to model imbalances, which could confine the impacts of assimilated ICs within a day. To address
25 this challenge, we introduce an Initial Error Transport Model (IETM) approach to improving $\text{PM}_{2.5}$
26 forecasts. The model describes the transport of initial errors by advection, diffusion, and decay
27 processes, and calculates the impacts of assimilated ICs separately from the CTM. The CTM
28 forecasts with unassimilated ICs are then corrected by the IETM output. We implement our method
29 to improve $\text{PM}_{2.5}$ forecasts over central and eastern China. The reduced root-mean-square errors
30 for 1- to 4-day forecasts during January 2018 are 51.2, 27.0, 16.4, and 9.4 $\mu\text{g m}^{-3}$, respectively,
31 which are 3.2, 6.9, 8.6, and 10.4 times those by the CTM forecasts with assimilated ICs. More
32 pronounced improvements are found for highly reactive $\text{PM}_{2.5}$ components. These and similar
33 results for July 2017 suggest that our method can enhance and extend the impacts of the assimilated
34 data without being affected by the imbalance issue.

35 INTRODUCTION

36 Air quality forecasting is essential for developing short-term air pollution control strategies and
37 mitigating health risks from air pollution.¹ Substantial forecast errors, however, may be induced
38 by uncertainties in the initial concentrations, emissions, and physical and chemical processes,
39 possibly leading to false alarms or missed episodes of pollution events.² Owing to the fast
40 economic growth and implementation of increasingly stringent emission control policies in China,
41 the rapid changes in emissions are usually not captured by the slowly updated emission inventories,
42 posing further challenges to air quality forecasting in China.³

43 Various data assimilation techniques, including optimal interpolation (OI),⁴ four-dimensional
44 variational assimilation (4D-Var),⁵ and ensemble Kalman filter (EnKF),⁶ have been adopted to
45 improve air quality forecasts. It is standard practice to supply initial conditions (ICs) directly to a
46 chemical transport model (CTM) with the assimilated data.⁷ This assimilated model initialization
47 approach has proved effective in improving air quality forecasts by assimilating diverse types of
48 observations such as in situ, remote sensing, and satellite data.⁸⁻¹⁰ Despite these considerable
49 successes, the benefits of data assimilation may not be fully exploited. Ma et al.¹¹ assimilated
50 surface in situ PM_{2.5} observations to improve 3-day PM_{2.5} forecasts and found that most
51 improvements by the assimilated ICs were limited to within the first day of the forecast; similar
52 conclusions were drawn from other studies when only surface PM_{2.5} observations are
53 assimilated.^{12,13} By contrast, it is estimated that the global average residence time of accumulation-
54 mode aerosols (0.1-2 μm diameter) emitted near the surface falls in the range of three to seven

55 days.^{14,15} This discrepancy between the residence time of aerosols and the duration of the impacts
56 of assimilated ICs suggests that PM_{2.5} forecasts can be further improved.

57 There are two types of imbalances that have hindered the improvement by using assimilated ICs
58 for model initialization. First, the number of assimilated species is often limited, resulting in the
59 imbalance between the assimilated and unassimilated variables.¹⁶ Also, the incomplete vertical
60 coverage of the assimilated data (e.g., by assimilating only surface observations) may lead to the
61 imbalance in space.¹⁷ By model initialization, these imbalances will be brought into the CTM and
62 generate spurious species interactions and vertical transport, which in turn degrade the forecasting
63 performance.¹⁸ Although this model imbalance issue is rarely discussed in the air quality
64 forecasting literature, some previous studies have indicated that PM_{2.5} forecasts can be improved
65 by extracting more observational information across space and chemical species. For example,
66 Schwartz¹⁹ showed that better forecasts were achieved by simultaneously assimilating surface
67 PM_{2.5} observations and satellite aerosol optical depth (AOD) retrievals. Moreover, it has been
68 found that 2- to 3-day forecasts of PM_{2.5} can be significantly improved by assimilating multi-
69 species surface chemical observations (e.g., PM_{2.5}, SO₂, and NO₂).^{8,20}

70 Model imbalances due to initialization, or initialization shocks, have been well recognized and
71 explored in numerical weather prediction and ocean modeling.^{21,22} Several procedures to mitigate
72 the initialization shock and increase the dynamical balance have been developed. These include,
73 among others, pre- and post-processing methods such as nonlinear normal mode initialization^{23,24}
74 and digital filtering,²⁵ as well as incremental analysis update schemes that gradually introduce the

75 analysis increments over a time window.²⁶ Although these initialization techniques are effective
76 in reducing spurious high-frequency oscillations, they do not completely eliminate the imbalances
77 and can partially undo the efforts of data assimilation.^{27,28}

78 In this study, we suggest a new way to extract information from the assimilated ICs without
79 bringing the imbalances into the CTM, and introduce an Initial Error Transport Model (IETM)
80 approach to improving PM_{2.5} forecasts. The model describes the transport of errors from the ICs
81 by advection, diffusion, and decay processes, and calculates the impacts of assimilated ICs
82 separately from the CTM. The CTM forecasts with unassimilated ICs are then corrected by the
83 IETM output. We implement and test our method on PM_{2.5} forecasts over central and eastern China
84 during January 2018 and July 2017. The reductions in root-mean-square error (RMSE) for 4-day
85 forecasts were still apparent, substantially improving results from direct initialization of the CTM.
86 Reasons that explain the improvements are also discussed.

87 **METHODS AND DATA**

88 **IETM Methodology**

89 Our model for describing the transport of initial errors is motivated by the fundamental principles
90 and major components of the governing equations for CTMs. A generic form of the governing
91 equation for a pollutant of interest is given by

$$92 \quad \frac{\partial c^f}{\partial t} = \nabla \cdot (K^f \nabla c^f) - \nabla \cdot (\mathbf{v}^f c^f) + E^f + R^f(c^f) + D^f(c^f) \quad (1)$$

93 where c^f is the pollutant concentration, K^f is the eddy diffusivity, \mathbf{v}^f is the wind vector, and E^f ,
94 R^f , and D^f are the changes of concentrations resulting from the emission, reaction, and deposition

95 processes, respectively. Here the superscript “f” stands for “forecast.” Equation 1 explicitly models
 96 the diffusion and advection processes, while leaving the other components nominally defined. Air
 97 quality forecasts are then obtained by solving the equation numerically with appropriate ICs.
 98 Conventionally, assimilated ICs with less bias and higher accuracy are supplied directly to the
 99 CTM. This approach, however, also brings imbalances in the assimilated ICs into the CTM,
 100 resulting in model imbalances and limiting the benefits of assimilated ICs.

101 We next derive a governing equation for the forecast errors. Suppose that the true concentrations
 102 follow the same form of governing equation as eq 1:

$$103 \quad \frac{\partial c^*}{\partial t} = \nabla \cdot (K^* \nabla c^*) - \nabla \cdot (\mathbf{v}^* c^*) + E^* + R^*(c^*) + D^*(c^*) \quad (2)$$

104 Define the forecast error by $e = c^f - c^*$. To obtain an equation in terms of e only, we assume for
 105 simplicity that the eddy diffusivity and the wind vector are without error, that is, $K^f = K^*$ and \mathbf{v}^f
 106 $= \mathbf{v}^*$. In the presence of errors in K^f and \mathbf{v}^f , the resulting equation will still be a good
 107 approximation, provided that these errors are relatively small. This assumption is reasonable, since
 108 diffusion is negligibly slow compared to advection²⁹ and wind forecasts are sufficiently accurate
 109 for up to 4 days.³⁰ Now, subtracting eq 2 from eq 1 gives the equation for the forecast error e :

$$110 \quad \frac{\partial e}{\partial t} = \nabla \cdot (K^f \nabla e) - \nabla \cdot (\mathbf{v}^f e) + \Psi(c^f, c^*) \quad (3)$$

111 where

$$112 \quad \Psi(c^f, c^*) = E^f + R^f(c^f) + D^f(c^f) - E^* - R^*(c^*) - D^*(c^*)$$

113 The first and second terms on the right-hand side of eq 3 are the diffusion and advection operators,
 114 respectively, which reflect the transport of forecast errors. Here the transported error refers to the

115 error transported from the previous time step, which involves errors arising from all sources
116 including emission, reaction, and deposition. Meanwhile, the last term Ψ in eq 3 represents the
117 error arising from all uncertainties at the current time step. This part of error is generally difficult
118 to estimate because it depends on the unknown true emission, reaction, and deposition processes.
119 Fortunately, for $\text{PM}_{2.5}$ as a pollutant with a typical lifetime of 4 days in the lower troposphere,³¹
120 the error generated at a single time step is relatively small compared to the transported error, as we
121 will show in SI Figure S1 and the Results and Discussion section. A related work by Skachko et
122 al.³² found that transport plays a major role in describing the evolution of model error for data
123 assimilation.

124 Although an explicit expression of Ψ in eq 3 is not available, the physical and chemical removal
125 processes of the pollutant are expected to follow an exponential decay.³³ We thus approximate Ψ
126 by a decay term and arrive at the governing equation for our initial error transport model (IETM):

$$127 \quad \frac{\partial e}{\partial t} = \nabla \cdot (K^f \nabla e) - \nabla \cdot (\mathbf{v}^f e) - \alpha e \quad (4)$$

128 where α is a decay rate parameter that controls the lifetime of the forecast errors. This simplified
129 equation can then be solved numerically. Although eq 4 depends on e only, solving the equation
130 requires knowing the initial error $e_0 = c_0^f - c_0^*$. Since c_0^* is unknown, we estimate it by the
131 assimilated initial concentration. Finally, consider a baseline forecast c^f that is obtained by
132 solving eq 1 with unassimilated ICs. In view of the relation $e = c^f - c^*$ mentioned above, we
133 correct the baseline forecast by subtracting the solution e^i to eq 4 and obtain our final forecast

$$134 \quad c^i = c^f - e^i$$

135 where the superscript “i” stands for the IETM approach.

136 To recap, the proposed IETM approach describes the transport of initial errors through a
137 simplified governing equation consisting of diffusion, advection, and decay terms. The solution to
138 this equation is then used to correct the baseline forecast from the full CTM with unassimilated
139 ICs. Overall, the IETM methodology avoids breaking the model balances in the CTM by
140 calculating the impacts of assimilated ICs separately from the CTM, thereby improving the final
141 forecasts.

142 **Numerical Implementation**

143 We adopted the Nested Air Quality Prediction Modeling System (NAQPMS)³⁴ developed by the
144 Institute of Atmospheric Physics, Chinese Academy of Sciences, as the CTM in this study.
145 NAQPMS runs in three dimensions with 20 vertical layers; more details about NAQPMS are
146 provided in Supporting Information (SI) Section S1. We used the method of optimal interpolation
147 (OI) for data assimilation, which is described in SI Section S2. Differences between the
148 unassimilated and assimilated ICs are treated as the ICs for the IETM. Numerical schemes and
149 parameter settings for implementing the advection, diffusion, and decay processes in eq 4 are
150 described as follows.

151 The advection process is calculated through a mass conservative, peak-preserving, mixing ratio
152 bounded advection algorithm developed by Walcek and Aleksic.³⁵ The algorithm employs dual-
153 linear segment approximations and a special treatment near the local maxima and minima to
154 preserve extremes and reduce numerical diffusion. It has been widely used in CTMs to advect

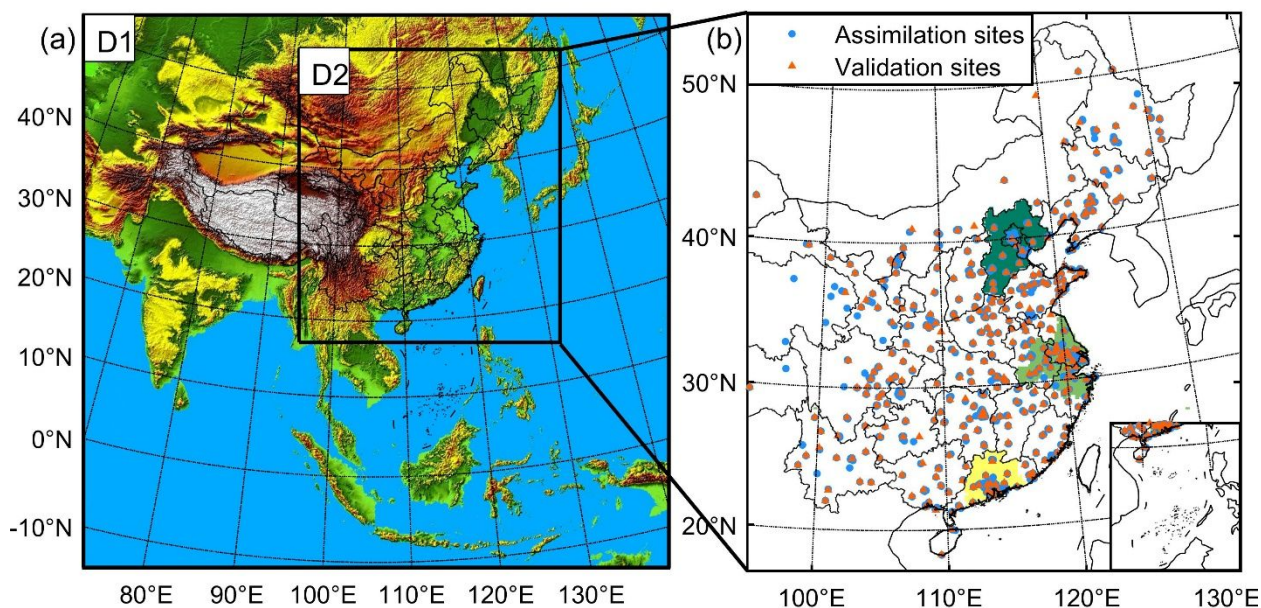
155 chemical species with nonnegative concentrations;^{34,36,37} however, it does not require positive-
156 definite initial fields, and negative quantities can be advected. A two-dimensional implementation
157 of the scheme is described in SI Section S3 and applied for the horizontal advection of forecast
158 errors. Vertical advection is not considered here for three reasons. First, only surface in situ
159 observations are assimilated in this study, so that the assimilated concentrations in the surface layer
160 are more accurate than those in higher layers. Second, vertical wind speeds are significantly
161 smaller than horizontal wind speeds. Finally, omitting the vertical advection would introduce a
162 relatively small error, but can save almost 90% of the computational cost.

163 The implementation of the diffusion process is straightforward except for determining the value
164 of eddy diffusivity K^f . Sometimes, K^f is set to zero or an empirical constant because diffusion is
165 negligibly slow compared to advection.²⁹ Here, it is calculated by a scheme based on model
166 resolution and wind speed derivatives.³⁸

167 The decay rate parameter α in eq 4 determines the lifetime of forecast errors. It has been shown
168 that the lifetimes of components in $PM_{2.5}$ range from less than a day to a few weeks.¹⁴ Here, we
169 regard the lifetime of the impacts of initial errors as the same as the lifetime of $PM_{2.5}$, which is
170 about 4 days in the lower troposphere.³¹ Accordingly, α is set to the reciprocal of the lifetime,
171 that is, $1/96 \text{ h}^{-1}$. As a result, the impacts of initial errors will last at least 4 days if not transported
172 outside the simulation domain.

173 During forecasting, we run the full CTM once to obtain the baseline forecast, and run the IETM
174 once to yield the correction. Compared with the conventional method that runs the CTM once with

175 assimilated ICs, our method requires extra computation to run the IETM. However, the IETM is a
176 two-dimensional, simplified model, which is easy and cheap to implement. Moreover, since the
177 background forecast has already been obtained in the OI assimilation scheme, it can be used
178 directly as the baseline forecast, thereby saving even more computation.



179 **Figure 1.** (a) Domain configurations and (b) distribution of monitoring sites. The outer domain
180 (D1) covers East Asia at a 45 km horizontal resolution, and the inner domain (D2) covers central
181 and eastern China at a 15 km horizontal resolution. Colored regions in (b) indicate the Beijing-
182 Tianjin-Hebei, Yangtze River Delta, and Pearl River Delta regions from north to south.

184

185 **Observational Data**

186 The surface $PM_{2.5}$ observations used in this study were obtained from the China National
187 Environmental Monitoring Center. These observations were first examined by a probabilistic
188 automatic outlier detection method³⁹ to remove data with abnormally large representation or

189 observational errors. After excluding sites with excessive missing or removed data, there were
190 1326 monitoring sites located in the research area as shown in Figure 1. Most of these sites were
191 in urban areas and there was more than one monitoring site for most cities. To ensure that there
192 was at least one assimilation site for each city, one validation site was randomly selected for cities
193 with more than two available sites. A total of 1003 sites were selected for assimilation, among
194 which 57 were located in the Beijing-Tianjin-Hebei (BTH) region, 120 in the Yangtze River Delta
195 (YRD) region, and 59 in the Pearl River Delta (PRD) region. The other 323 sites were used for
196 validation, including 13, 37, and 15 sites in the BTH, YRD, and PRD region, respectively.

197 **Configurations of Forecasting Experiments**

198 Three forecasting experiments were carried out to produce 96 h forecasts of $PM_{2.5}$ during
199 January 2018 and July 2017. These experiments share the same domain configurations, emission
200 inventories, meteorological initial and boundary conditions, and parameter settings for the CTM,
201 with the only difference being the treatments of ICs as described below.

202 The first experiment supplies the unassimilated ICs, which are extracted from the forecasts
203 started 24 h ago, directly to the CTM. The second experiment uses the assimilated ICs instead for
204 the CTM. The third experiment implements the proposed method, which corrects the forecasts
205 produced in the first experiment with the output from the IETM. The ICs for the IETM are obtained
206 by subtracting the assimilated ICs from the unassimilated ICs. While the CTM includes 20 vertical
207 layers, only surface $PM_{2.5}$ observations were obtained and assimilated in this study. The restart
208 interval is set to 24 h and the assimilation frequency is hourly. Components of $PM_{2.5}$ in the

209 assimilated ICs (e.g., nitrate, sulfate, organic aerosols, and black carbon) are adjusted
210 proportionally to the change of total $\text{PM}_{2.5}$ before and after data assimilation.

211 **RESULTS AND DISCUSSION**

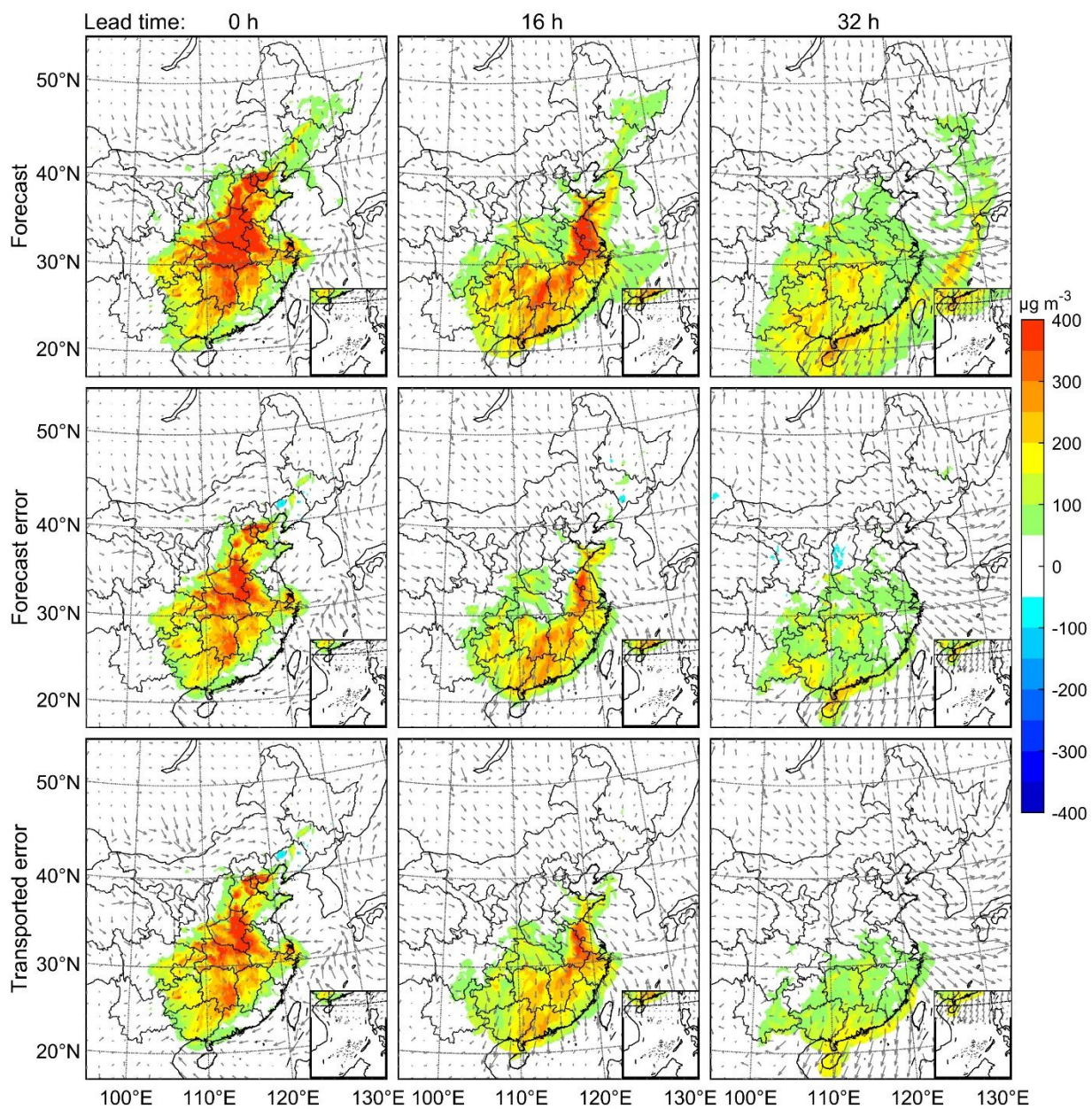
212 **Transport of Forecast Errors**

213 It is well documented that transport plays a major role in the evolution of $\text{PM}_{2.5}$.⁴⁰⁻⁴² The $\text{PM}_{2.5}$
214 driven by cold surges can travel up to 2000 km from northern to southern China within two days.⁴³
215 Moreover, components with longer lifetimes (e.g., dust and black carbon) can travel across
216 oceans,⁴⁴ and intercontinental transport of aerosols is estimated to account for 36–97% of the
217 background surface concentrations.⁴⁰

218 Equation 3 suggests that the forecast errors of $\text{PM}_{2.5}$ can be similarly transported. Numerical
219 evidence for such error transport from the forecasting experiments is shown in Figure 2 and SI
220 Video S1. At the beginning of the forecast period, $\text{PM}_{2.5}$ concentrations above $300 \mu\text{g m}^{-3}$ are
221 found in Henan, Hebei, Hunan, and Hubei. During the forecast, most $\text{PM}_{2.5}$ is transported to the
222 Pacific Ocean by a strong northwest wind. At the lead time of 32 h, $\text{PM}_{2.5}$ concentrations for most
223 of the Chinese mainland fall below $150 \mu\text{g m}^{-3}$, as shown in the top panel of Figure 2. For
224 comparison, we estimated the forecast errors by the difference between the forecast and the
225 assimilated concentrations, as shown in the middle panel of Figure 2. Accuracy of the assimilated
226 data is verified in SI Section S4 and Figure S2. As is clear from Figure 2, forecast errors are
227 transported along with concentrations, and large forecast errors occur mostly in heavily polluted
228 areas. The transported initial errors, calculated by using the IETM approach, are shown in the

229 bottom panel of Figure 2. The estimated forecast errors and the transported initial errors are
230 identical by definition at the start of the forecast. During the forecast, the differences increase, but
231 the transported errors consistently account for most of the estimated errors. The differences are
232 likely attributable to uncertainties in the emissions, reactions, deposition, and wind fields. To sum
233 up, these results confirm that forecast errors of $PM_{2.5}$ can be transported along with concentrations
234 from the CTM and the transported errors have a strong impact on forecasts with a lead time up to
235 32 h.

236 To further demonstrate the importance of transport in the evolution of forecast errors, we
237 decompose the forecast errors into two parts: the error transported from an hour ago and the other
238 error that is generated during the last hour. Both parts of error involve uncertainties stemming from
239 the CTM modules and the input data, thus forming a different decomposition from those usually
240 discussed in the literature. As shown in SI Figure S1, the transported error outweighs the other
241 error by a factor of 6.6. This result is consistent with the work of Skachko et al.,³² which found
242 that transport plays a major role in describing the evolution of model error for data assimilation.



243

244 **Figure 2.** Illustrations of the transport of $\text{PM}_{2.5}$ forecast errors. The forecast starts at 20:00 on
245 January 6, 2018. Forecast errors (middle) are estimated by the difference between the forecast (top)
246 and assimilated concentrations. Transported errors (bottom) are calculated by using the IETM
247 approach. An animated version of this figure is provided in SI Video S1.

248

249 **Comparisons of Forecasting Methods**

250 We compare the proposed IETM method with two commonly used forecasting schemes
251 mentioned above, which we refer to as CTM forecasting with unassimilated ICs (CTMf) and that
252 with assimilated ICs (CTMa). Three statistical measures are used to evaluate the accuracy of the
253 forecasts: mean bias (MB), root-mean-square error (RMSE), and correlation coefficient (r).
254 Results for 1- to 4-day PM_{2.5} forecasts during January 2018 using three methods over the study
255 period are summarized in Table 1. Examples of the forecast PM_{2.5} concentrations at three
256 validation sites in the BTH, YRD, and PRD regions are shown in SI Figure S3.

257 As noted from Table 1, the CTMf method exhibits a large upward bias of 57.0–64.0 $\mu\text{g m}^{-3}$ for
258 1- to 4-day forecasts over all validation sites. This overestimation could be largely explained by
259 stringent emission controls that are not captured by the currently used emission inventory, such as
260 strengthening industrial emissions standards, upgrading industrial boilers, phasing out outdated
261 industrial capacities, and promoting clean fuels in the residential sector.

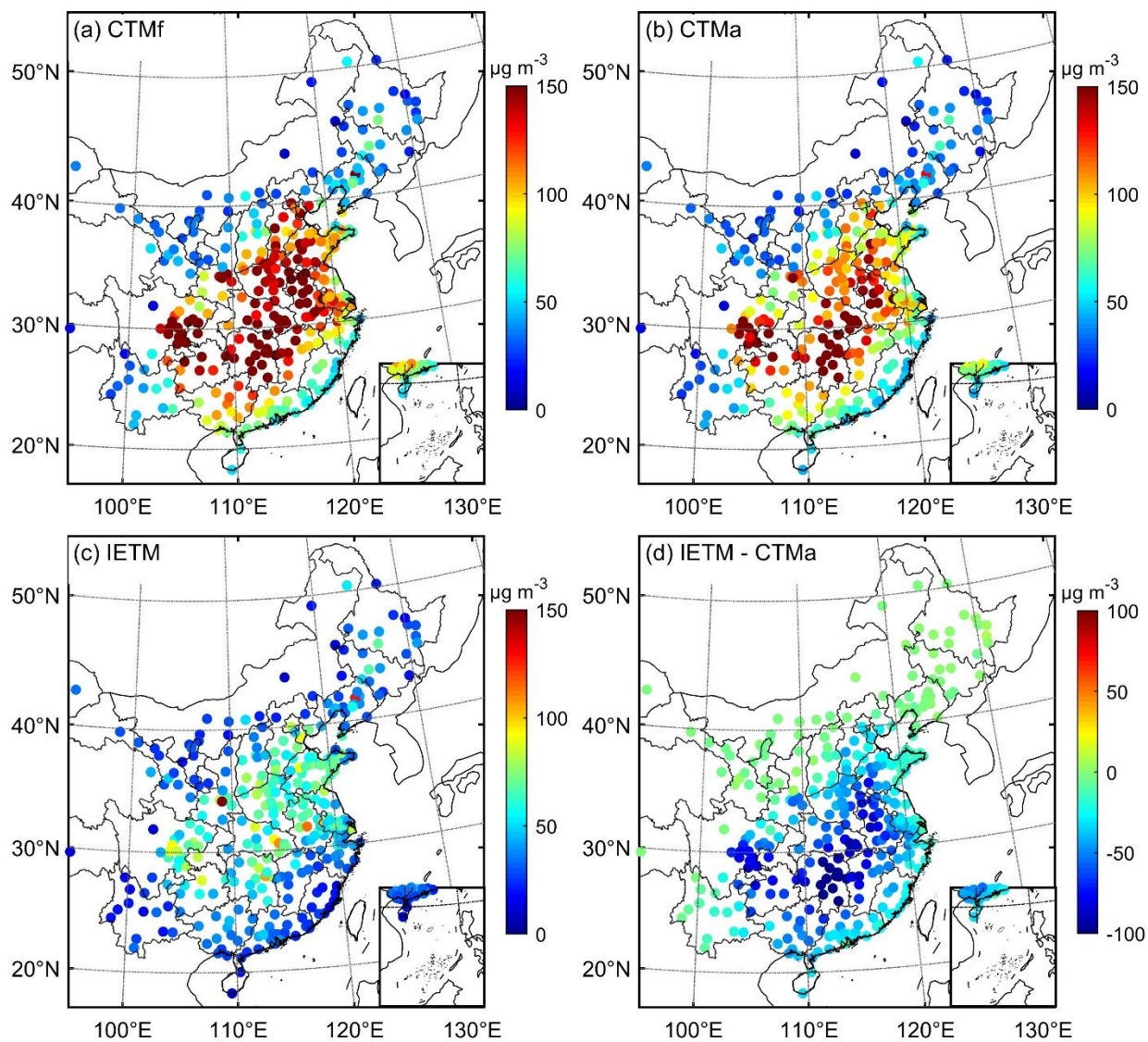
262 **Table 1. Performance Statistics for 1- to 4-Day PM_{2.5} Forecasts During January 2018 Using**
 263 **Three Methods^a**

region	method	1-day forecast			2-day forecast			3-day forecast			4-day forecast		
		MB	RMSE	<i>r</i>	MB	RMSE	<i>r</i>	MB	RMSE	<i>r</i>	MB	RMSE	<i>r</i>
all	CTMf	64.0	98.9	0.43	59.8	97.5	0.39	59.3	98.3	0.36	57.0	98.3	0.31
	CTMa	51.3	82.6	0.47	57.0	93.6	0.40	58.0	96.4	0.36	56.4	97.4	0.31
	IETM	15.8	47.7	0.58	31.1	70.5	0.39	41.9	81.9	0.34	47.2	88.9	0.29
BTH	CTMf	66.7	111.5	0.54	64.1	109.2	0.49	70.1	115.4	0.41	66.6	119.9	0.33
	CTMa	48.9	86.7	0.59	62.1	105.7	0.49	69.4	114.1	0.41	66.3	119.4	0.33
	IETM	22.6	60.5	0.61	51.2	94.3	0.46	64.9	108.4	0.41	64.4	117.1	0.33
YRD	CTMf	78.1	112.4	0.68	70.1	113.8	0.61	67.0	122.2	0.50	66.3	121.2	0.47
	CTMa	62.8	92.8	0.71	67.3	109.6	0.62	65.7	120.2	0.50	65.7	120.2	0.47
	IETM	21.5	53.1	0.73	38.6	81.2	0.60	51.9	103.6	0.48	58.6	110.0	0.46
PRD	CTMf	49.1	76.4	0.20	47.7	75.1	0.20	48.2	78.5	0.21	49.3	81.1	0.18
	CTMa	41.3	66.7	0.27	44.2	70.9	0.22	46.4	76.0	0.21	48.3	79.6	0.17
	IETM	1.6	34.8	0.60	-5.3	47.4	0.18	4.7	55.4	0.04	20.5	63.6	0.07

264 ^aBTH, Beijing-Tianjin-Hebei region; YRD, Yangtze River Delta region; PRD, Pearl River Delta
 265 region. MB, mean bias ($\mu\text{g m}^{-3}$); RMSE, root-mean-square error ($\mu\text{g m}^{-3}$); *r*, correlation
 266 coefficient. The CTMf and CTMa methods refer to CTM forecasting with unassimilated and
 267 assimilated ICs, respectively, and IETM refers to CTMf corrected by the IETM output.

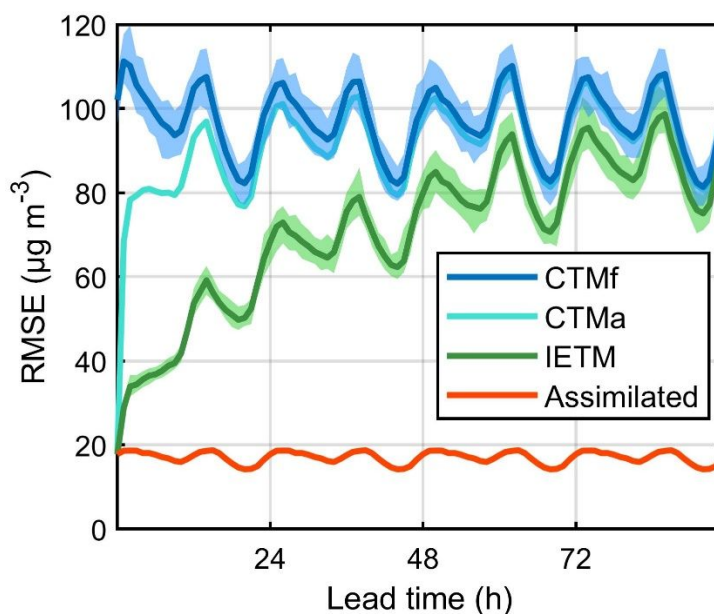
268
 269 The CTMa method yields improved forecasting performance over CTMf by initializing the CTM
 270 with the assimilated data. As shown in Figure 3, the RMSE of 1-day forecasts using the CTMf
 271 method exceeds $150 \mu\text{g m}^{-3}$ at most validation sites in the Sichuan Basin, the North China Plain,
 272 and the Hubei–Hunan Plain, while RMSEs under $50 \mu\text{g m}^{-3}$ are found mainly in Northeast China,

273 Northwest China, and Yunnan. A reduction of RMSE is clearly observed in areas with high
274 RMSEs, especially the North China Plain. The RMSE of 1-day forecasts over all validation sites
275 is lowered by $16.2 \mu\text{g m}^{-3}$, amounting to a reduction of 16.4% (Table 1).



276
277 **Figure 3.** Maps of RMSE at validation sites for 1-day forecasts during January 2018. The RMSEs
278 of the CTMf, CTMa, and IETM methods are shown in (a)–(c), respectively, and differences
279 between the RMSEs of IETM and CTMa are shown in (d).

280



281
282 **Figure 4.** Curves of RMSE over all validation sites as functions of lead time for PM_{2.5} forecasts
283 during January 2018. Shaded areas around the curves for CTMa and IETM represent 95%
284 confidence intervals, which are calculated by using the bootstrap method. The red line represents
285 the RMSE of assimilated PM_{2.5} from the CTM.

286
287 Although PM_{2.5} forecasts are generally improved by the CTMa method, the benefits are largely
288 limited to 1-day forecasts. At the beginning of the forecast, the RMSE for the CTMa method is
289 substantially lower than that for CTMf, as evident from Figure 4. However, the RMSE for CTMa
290 increases dramatically and its advantage over CTMf is quickly lost, especially during the first hour.
291 A similar phenomenon in the first hour of the forecast was also noted by previous work,¹⁹ where
292 only observations of PM_{2.5}, but not its precursors, were assimilated. Compared with the relatively
293 large improvement for 1-day forecasts, only reductions of 3.9, 1.9, and 0.9 µg m⁻³, or 4.0%, 1.9%,

294 and 0.9%, respectively, are obtained from the CTMa method for 2- to 4-day forecasts (Table 1).
295 These results are consistent with previous studies suggesting that most improvements by
296 assimilating surface PM_{2.5} observations are limited to 1-day forecasts.¹¹⁻¹³

297 By contrast, improvements from the IETM method tend to be more substantial and last longer.
298 Starting with the same reduction in RMSE as that by CTMa, the IETM forecasts only see a gradual
299 increase in RMSE during the first two days, and the impacts of assimilated ICs are still visible on
300 the fourth day in Figure 4. A periodic diurnal variation in the RMSEs of all forecasts is noted in
301 Figure 4, which is likely caused by uncertainties in the diurnal variation of emissions and
302 meteorological conditions such as solar intensity, temperature, wind speed, and the height of the
303 planetary boundary layer. As shown spatially in Figure 3, improvements in RMSE for 1-day
304 forecasts by IETM over CTMa are apparent at most validation sites and more pronounced in areas
305 with high RMSEs. Remarkably, while the RMSEs for validation sites in Guangdong, Fujian, and
306 Zhejiang are scarcely reduced by CTMa, they are cut down to under 50 $\mu\text{g m}^{-3}$ by the IETM
307 method. Compared with the results for CTMf, the reductions in RMSE for 1- to 4-day forecasts
308 by the IETM method are 51.2, 27.0, 16.4, and 9.4 $\mu\text{g m}^{-3}$, or 51.8%, 27.7%, 16.7%, and 9.5%,
309 respectively, which are 3.2, 6.9, 8.6, and 10.4 times those by the CTMa method (Table 1). Table
310 1 also suggests that improvements by the IETM method are mainly in the MB and RMSE but less
311 in the correlation coefficient, especially for 2- to 4-day forecasts. This inconsistency is due to the
312 fact that r is a standardized measure that magnifies the contributions of locations with low
313 concentrations and hence small forecast errors. The IETM approach, however, tends to transport

314 large forecast errors to locations with small errors, which may decrease r for those locations and
315 offset the improvement in r elsewhere. Nevertheless, since $\text{PM}_{2.5}$ concentrations and forecast
316 errors show marked spatiotemporal variability, the MB and RMSE measures seem more
317 appropriate for assessing predictive accuracy in this case.

318 To further test the robustness of our method for different periods and seasons, we applied it to
319 the month of July 2017. Although the RMSE is much lower in the summer, the results show similar
320 trends of improvement to those for January 2018. Notably, as shown in SI Figure S4, the RMSEs
321 for 1-day forecasts in the Sichuan Basin are only slightly reduced by the CTMa method, but are
322 cut by about a half with the IETM method. The reduced RMSEs for 1- to 4-day forecasts during
323 July 2017 and January 2018 are compared in SI Figure S5, which demonstrate similar patterns and
324 last up to 4 days. These results together suggest that the IETM method can yield amplified and
325 prolonged improvement over commonly used forecasting schemes.

326 **Model Balances in the Forecasts**

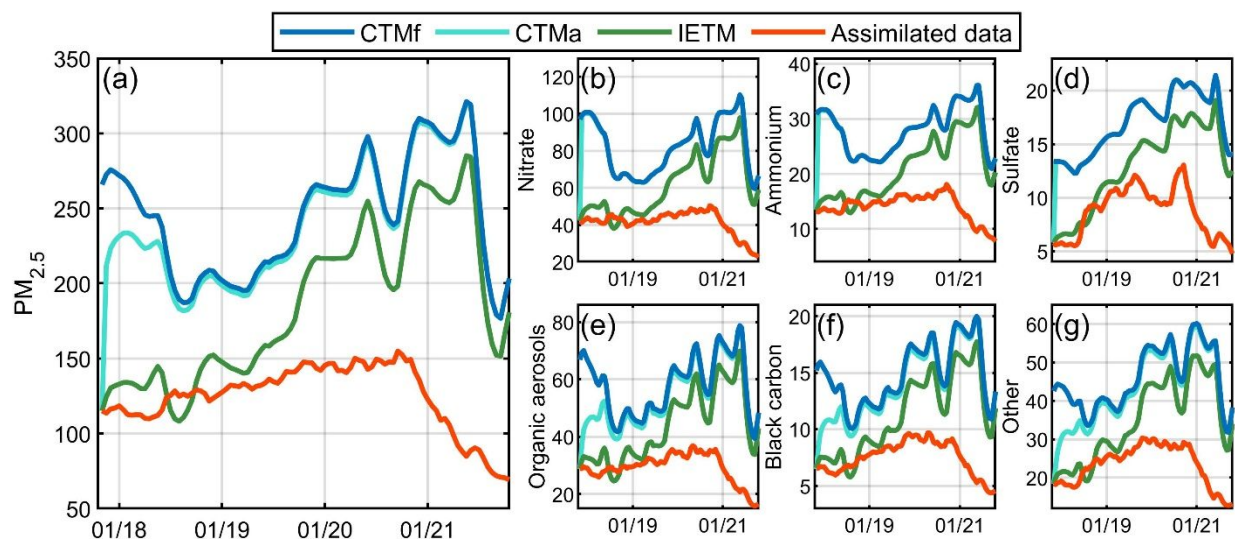
327 It is useful to investigate the ways in which the proposed IETM method helps to mitigate the
328 imbalance issue. Two types of imbalances can generally occur in the CTM due to data assimilation.
329 The first type is the imbalance between the assimilated and unassimilated model variables.¹⁶
330 Ideally, the calculation of chemical reactions should be more accurate with the assimilated ICs. In
331 reality, however, only a few of the species involved in the CTM can be assimilated owing to the
332 lack of observations. This inconsistency can thus disturb the balance of chemical reactions. As a
333 result, improvements for the assimilated species may diminish quickly as the CTM tries to reach

334 a new reaction balance. The second type is the imbalance in space.¹⁷ For instance, in this study,
335 the accuracy of ICs in the surface layer was improved by assimilating surface $PM_{2.5}$ observations,
336 whereas $PM_{2.5}$ in the higher layers was not affected since no lidar or satellite data were assimilated.
337 Such an imbalance may lead to spurious differences between the concentrations of $PM_{2.5}$ in the
338 surface layer and in the adjacent layer. During the forecast, these spurious differences tend to be
339 lessened by vertical transport in the CTM; however, the effects of data assimilation on surface
340 $PM_{2.5}$ are also counteracted. Collectively, these two types of imbalances may cause spurious
341 species interactions and vertical transport in the CTM, thereby diminishing the benefits from data
342 assimilation.

343 The IETM method takes a fundamentally different way to extract information from the
344 assimilated ICs. It calculates the transport of initial errors and corrects the baseline forecast
345 accordingly. Neither of the two imbalance problems mentioned above will be encountered. First,
346 the IETM does not explicitly involve any reaction process, thereby avoiding interactions between
347 the assimilated and unassimilated species. Moreover, only the surface layer is considered in the
348 IETM, so that no vertical imbalance will arise.

349 To verify the above arguments, we estimated the concentrations of $PM_{2.5}$ components using the
350 IETM by assuming that the chemical composition of $PM_{2.5}$ is the same as that in the baseline CTM
351 forecast. Results averaged over the YRD region for a 4-day period are shown in Figure 5. Since
352 no precursors of $PM_{2.5}$ were assimilated in this study, chemical reactions between $PM_{2.5}$
353 components and their precursors were significantly disturbed in the CTMa method. As expected,

354 the concentrations of highly reactive PM_{2.5} components, including nitrate, ammonium, and sulfate,
355 change abruptly in the first hour and become indistinguishable from the CTMf forecasts (Figure
356 5b–d). By contrast, improvements for these components by the IETM method are consistently
357 large and can last up to four days. Similar trends are found for those less reactive components,
358 including organic aerosols, black carbon, and other PM_{2.5} components (Figure 5e–g). In this case,
359 it is interesting to note that, although the CTMa forecasts converge to those by CTMf and the
360 effects of data assimilation almost disappear within a day, the changes are not as abrupt as those
361 for highly reactive components. This difference suggests that vertical transport may play a major
362 role for these components, which takes a longer time to reach a dynamic balance. The relatively
363 longer duration of assimilation effect may also be attributed to the start time of 20:00 and weaker
364 vertical transport in the nighttime. In summary, improvements by the IETM method are substantial
365 and consistent across all components of PM_{2.5}, and are not affected by either spurious species
366 interactions or vertical transport.



367

368 **Figure 5.** Time series of the CTMf, CTMa, and IETM forecasts of total PM_{2.5} (a) and its
369 components (b–g) over the Yangtze River Delta region. The forecast starts at 20:00 on January 17,
370 2018.

371 Limitations and Possible Extensions

372 Fully exploiting the benefits of data assimilation is crucial for improving air quality forecasting.
373 Our proposed method provides a reliable, flexible way to enhance and extend the impacts of the
374 assimilated data without being affected by the imbalance issue. The methodology is easy to
375 implement and highly efficient as it does not require expensive CTM computations or complex
376 initialization strategies. Nevertheless, the IETM assumes that the lifetime of PM_{2.5} forecast errors
377 is prespecified and vertical transport is negligible. Although these assumptions affect only the
378 calculated impacts of assimilated ICs and seem plausible in most cases, there are exceptions. For
379 instance, scavenging of PM_{2.5} by precipitation would result in a shorter lifetime of PM_{2.5}. Besides,
380 when air masses collide or wildfires occur, vertical transport may play a more important role and

381 should not be ignored. Moreover, since the IETM trades model complexity for model balance, its
382 advantages over direct initialization techniques would diminish as the number of species and
383 vertical coverage in the assimilated data increase.

384 The IETM method could be extended in many ways to deal with these limitations. For example,
385 a more sophisticated decay scheme, incorporating the reaction and deposition processes, could be
386 developed, which would provide better predictions over areas and periods with unusual $PM_{2.5}$
387 lifetimes. Moreover, the forecast errors that are not explained by the transport or decay of initial
388 errors could be modeled using statistical or machine learning methods, which is likely to yield
389 further improvement for longer-range forecasts.

390 ASSOCIATED CONTENT

391 **Supporting Information**

392 Detailed descriptions of the CTM and data assimilation method, implementation of horizontal

393 advection, validation of assimilation results, supplementary figures (PDF)

394 Animation of the transport of PM_{2.5} forecast errors (Video S1) (AVI)

395 AUTHOR INFORMATION

396 **Corresponding Authors**

397 *Email: wuhuangjian@pku.edu.cn

398 *Email: weilin@math.pku.edu.cn

399 **Notes**

400 The authors declare no competing financial interest.

401 ACKNOWLEDGMENTS

402 This work was supported by National Key R&D Program of China grants 2016YFC0207703,

403 2016YFC0207701, 2018YFC0213106, and 2018YFC0213100, National Natural Science

404 Foundation of China grants 11671018, 71532001, 91644216, and 41705108, Beijing Natural

405 Science Foundation grant Z190001, and Beijing Academy of Artificial Intelligence.

406 REFERENCES

- 407 (1) Zhang, Y.; Bocquet, M.; Mallet, V.; Seigneur, C.; Baklanov, A. Real-time air quality
408 forecasting, part I: History, techniques, and current status. *Atmos. Environ.* **2012**, *60*, 632-655.
- 409 (2) Kumar, R.; Peuch, V.-H.; Crawford, J. H.; Brasseur, G. Five steps to improve air-quality
410 forecasts. *Nature* **2018**, *561* (7721), 27-29.
- 411 (3) Zhang, Q.; Zheng, Y.; Tong, D.; Shao, M.; Wang, S.; Zhang, Y.; Xu, X.; Wang, J.; He, H.;
412 Liu, W.; Ding, Y.; Lei, Y.; Li, J. H.; Wang, Z.; Zhang, X.; Wang, Y.; Cheng, J.; Liu, Y.; Shi, Q.;
413 Yan, L.; Geng, G.; Hong, C.; Li, M.; Liu, F.; Zheng, B.; Cao, J.; Ding, A.; Gao, J.; Fu, Q.; Huo,
414 J.; Liu, B.; Liu, Z.; Yang, F.; He, K.; Hao, J. Drivers of improved PM_{2.5} air quality in China from
415 2013 to 2017. *Proc. Natl. Acad. Sci. U.S.A.* **2019**, *116* (49), 24463-24469.
- 416 (4) Daley, R., *Atmospheric Data Analysis*. Cambridge University Press: Cambridge, U.K.,
417 1991.
- 418 (5) Talagrand, O.; Courtier, P. Variational assimilation of meteorological observations with the
419 adjoint vorticity equation. I: Theory. *Q. J. R. Meteorol. Soc.* **1987**, *113* (478), 1311-1328.
- 420 (6) Evensen, G. Sequential data assimilation with a nonlinear quasi-geostrophic model using
421 Monte Carlo methods to forecast error statistics. *J. Geophys. Res.* **1994**, *99* (C5), 10143-10162.
- 422 (7) Bocquet, M.; Elbern, H.; Eskes, H.; Hirtl, M.; Žabkar, R.; Carmichael, G. R.; Flemming, J.;
423 Inness, A.; Pagowski, M.; Camaño, J. L. P.; Saide, P. E.; San Jose, R.; Sofiev, M.; Vira, J.;
424 Baklanov, A.; Carnevale, C.; Grell, G.; Seigneur, C. Data assimilation in atmospheric chemistry
425 models: current status and future prospects for coupled chemistry meteorology models. *Atmos.*
426 *Chem. Phys.* **2015**, *15* (10), 5325-5358.
- 427 (8) Peng, Z.; Lei, L.; Liu, Z.; Su, J.; Ding, A.; Ban, J.; Chen, D.; Kou, X.; Chu, K. The impact
428 of multi-species surface chemical observation assimilation on air quality forecasts in China.
429 *Atmos. Chem. Phys.* **2018**, *18* (23), 17387-17404.
- 430 (9) Cheng, X.; Liu, Y.; Xu, X.; You, W.; Zang, Z.; Gao, L.; Chen, Y.; Su, D.; Yan, P. Lidar
431 data assimilation method based on CRTM and WRF-Chem models and its application in PM_{2.5}
432 forecasts in Beijing. *Sci. Total Environ.* **2019**, *682*, 541-552.
- 433 (10) Saide, P. E.; Kim, J.; Song, C. H.; Choi, M.; Cheng, Y.; Carmichael, G. R. Assimilation of
434 next generation geostationary aerosol optical depth retrievals to improve air quality simulations.
435 *Geophys. Res. Lett.* **2014**, *41* (24), 9188-9196.
- 436 (11) Ma, C.; Wang, T.; Zang, Z.; Li, Z. Comparisons of three-dimensional variational data
437 assimilation and model output statistics in improving atmospheric chemistry forecasts. *Adv.*
438 *Atmos. Sci.* **2018**, *35* (7), 813-825.
- 439 (12) Li, Z.; Zang, Z.; Li, Q. B.; Chao, Y.; Chen, D.; Ye, Z.; Liu, Y.; Liou, K. N. A three-
440 dimensional variational data assimilation system for multiple aerosol species with WRF/Chem
441 and an application to PM_{2.5} prediction. *Atmos. Chem. Phys.* **2013**, *13* (8), 4265-4278.
- 442 (13) Feng, S.; Jiang, F.; Jiang, Z.; Wang, H.; Cai, Z.; Zhang, L. Impact of 3DVAR assimilation
443 of surface PM_{2.5} observations on PM_{2.5} forecasts over China during wintertime. *Atmos. Environ.*
444 **2018**, *187*, 34-49.

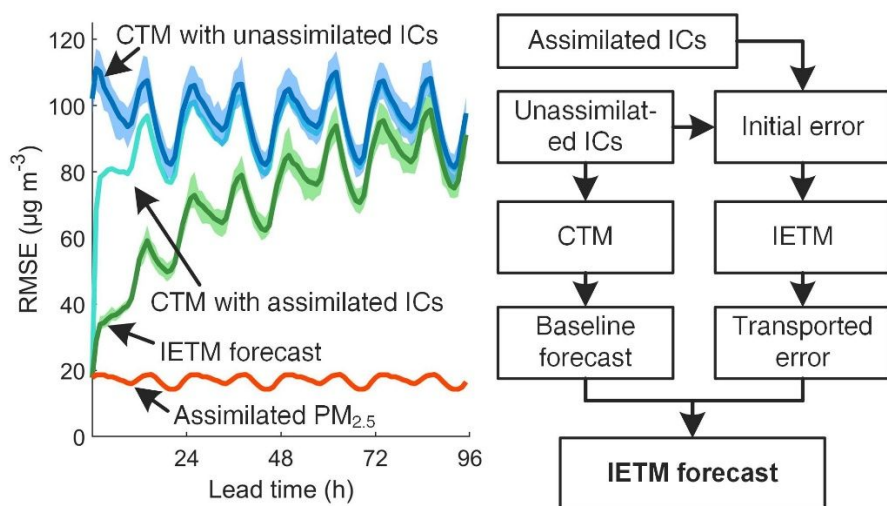
- 445 (14) Textor, C.; Schulz, M.; Guibert, S.; Kinne, S.; Balkanski, Y.; Bauer, S.; Bernsten, T.;
446 Berglen, T.; Boucher, O.; Chin, M.; Dentener, F.; Diehl, T.; Easter, R.; Feichter, H.; Fillmore,
447 D.; Ghan, S.; Ginoux, P.; Gong, S.; Grini, A.; Hendricks, J.; Horowitz, L.; Huang, P.; Isaksen, I.;
448 Iversen, I.; Kloster, S.; Koch, D.; Kirkevåg, A.; Kristjansson, J. E.; Krol, M.; Lauer, A.;
449 Lamarque, J. F.; Liu, X.; Montanaro, V.; Myhre, G.; Penner, J.; Pitari, G.; Reddy, S.; Seland, Ø.;
450 Stier, P.; Takemura, T.; Tie, X. Analysis and quantification of the diversities of aerosol life
451 cycles within AeroCom. *Atmos. Chem. Phys.* **2006**, *6* (7), 1777-1813.
- 452 (15) Croft, B.; Pierce, J. R.; Martin, R. V. Interpreting aerosol lifetimes using the GEOS-Chem
453 model and constraints from radionuclide measurements. *Atmos. Chem. Phys.* **2014**, *14* (8), 4313-
454 4325.
- 455 (16) Weaver, A. T.; Deltel, C.; Machu, E.; Ricci, S.; Daget, N. A multivariate balance operator
456 for variational ocean data assimilation. *Q. J. R. Meteorol. Soc.* **2005**, *131* (613), 3605-3625.
- 457 (17) Greybush, S. J.; Kalnay, E.; Miyoshi, T.; Ide, K.; Hunt, B. R. Balance and Ensemble
458 Kalman Filter Localization Techniques. *Mon. Weather Rev.* **2011**, *139* (2), 511-522.
- 459 (18) Carrassi, A.; Bocquet, M.; Bertino, L.; Evensen, G. Data assimilation in the geosciences:
460 An overview of methods, issues, and perspectives. *WIREs Clim. Change* **2018**, *9* (5), No. e535.
- 461 (19) Schwartz, C. S.; Liu, Z.; Lin, H.-C.; McKeen, S. A. Simultaneous three-dimensional
462 variational assimilation of surface fine particulate matter and MODIS aerosol optical depth. *J.*
463 *Geophys. Res.* **2012**, *117* (D13), No. D13202.
- 464 (20) Zheng, H.; Liu, J.; Tang, X.; Wang, Z.; Wu, H.; Yan, P.; Wang, W. Improvement of the
465 Real-time PM_{2.5} Forecast over the Beijing-Tianjin-Hebei Region using an Optimal Interpolation
466 Data Assimilation Method. *Aerosol Air Qual. Res.* **2018**, *18* (5), 1305-1316.
- 467 (21) Balmaseda, M.; Anderson, D. Impact of initialization strategies and observations on
468 seasonal forecast skill. *Geophys. Res. Lett.* **2009**, *36* (1), No. L01701.
- 469 (22) Mulholland, D. P.; Laloyaux, P.; Haines, K.; Balmaseda, M. A. Origin and Impact of
470 Initialization Shocks in Coupled Atmosphere–Ocean Forecasts. *Mon. Weather Rev.* **2015**, *143*
471 (11), 4631-4644.
- 472 (23) Machenhauer, B. On the Dynamics of Gravity Oscillations in a Shallow Water Model,
473 with Applications to Normal Mode Initialization. *Contrib. Atmos. Phys.* **1977**, *50*, 253-271.
- 474 (24) Baer, F.; Tribbia, J. J. On Complete Filtering of Gravity Modes Through Nonlinear
475 Initialization. *Mon. Weather Rev.* **1977**, *105* (12), 1536-1539.
- 476 (25) Lynch, P.; Huang, X.-Y. Initialization of the HIRLAM Model Using a Digital Filter. *Mon.*
477 *Weather Rev.* **1992**, *120* (6), 1019-1034.
- 478 (26) Bloom, S. C.; Takacs, L. L.; da Silva, A. M.; Ledvina, D. Data Assimilation Using
479 Incremental Analysis Updates. *Mon. Weather Rev.* **1996**, *124* (6), 1256-1271.
- 480 (27) Williamson, D. L.; Daley, R.; Schlatter, T. W. The Balance between Mass and Wind Fields
481 Resulting from Multivariate Optimal Interpolation. *Mon. Weather Rev.* **1981**, *109* (11), 2357-
482 2376.
- 483 (28) Errico, R. M.; Rosmond, T. E.; Goerss, J. S. A Comparison of Analysis and Initialization
484 Increments in an Operational Data-Assimilation System. *Mon. Weather Rev.* **1993**, *121* (2), 579-
485 588.

- 486 (29) Keller, C. A.; Evans, M. J. Application of random forest regression to the calculation of
487 gas-phase chemistry within the GEOS-Chem chemistry model v10. *Geosci. Model Dev.* **2019**, *12*
488 (3), 1209-1225.
- 489 (30) Bauer, P.; Thorpe, A.; Brunet, G. The quiet revolution of numerical weather prediction.
490 *Nature* **2015**, *525* (7567), 47-55.
- 491 (31) Kristiansen, N. I.; Stohl, A.; Olivié, D. J. L.; Croft, B.; Søvde, O. A.; Klein, H.;
492 Christoudias, T.; Kunkel, D.; Leadbetter, S. J.; Lee, Y. H.; Zhang, K.; Tsigaridis, K.; Bergman,
493 T.; Evangeliou, N.; Wang, H.; Ma, P.-L.; Easter, R. C.; Rasch, P. J.; Liu, X.; Pitari, G.; Di
494 Genova, G.; Zhao, S. Y.; Balkanski, Y.; Bauer, S. E.; Faluvegi, G. S.; Kokkola, H.; Martin, R.
495 V.; Pierce, J. R.; Schulz, M.; Shindell, D.; Tost, H.; Zhang, H. Evaluation of observed and
496 modelled aerosol lifetimes using radioactive tracers of opportunity and an ensemble of 19 global
497 models. *Atmos. Chem. Phys.* **2016**, *16* (5), 3525-3561.
- 498 (32) Skachko, S.; Ménard, R.; Errera, Q.; Christophe, Y.; Chabrillat, S. EnKF and 4D-Var data
499 assimilation with chemical transport model BASCOE (version 05.06). *Geosci. Model Dev.* **2016**,
500 *9* (8), 2893-2908.
- 501 (33) Liu, X.; Yeo, K.; Hwang, Y.; Singh, J.; Kalagnanam, J. A statistical modeling approach for
502 air quality data based on physical dispersion processes and its application to ozone modeling.
503 *Ann. Appl. Stat.* **2016**, *10* (2), 756-785.
- 504 (34) Wang, Z.; Maeda, T.; Hayashi, M.; Hsiao, L.-F.; Liu, K.-Y. A Nested Air Quality
505 Prediction Modeling System for Urban and Regional Scales: Application for High-Ozone
506 Episode in Taiwan. *Water Air Soil Pollut.* **2001**, *130* (1-4), 391-396.
- 507 (35) Walcek, C. J.; Aleksic, N. M. A simple but accurate mass conservative, peak-preserving,
508 mixing ratio bounded advection algorithm with Fortran code. *Atmos. Environ.* **1998**, *32* (22),
509 3863-3880.
- 510 (36) Jacobson, M. Z. GATOR-GCMM: A global- through urban-scale air pollution and weather
511 forecast model 1. Model design and treatment of subgrid soil, vegetation, roads, rooftops, water,
512 sea ice, and snow. *J. Geophys. Res.* **2001**, *106* (D6), 5385-5401.
- 513 (37) Kadowaki, M.; Katata, G.; Terada, H.; Nagai, H. Development of the Eulerian atmospheric
514 transport model GEARN-FDM: Validation against the European tracer experiment. *Atmos.*
515 *Pollut. Res.* **2017**, *8* (2), 394-402.
- 516 (38) Smagorinsky, J. General circulation experiments with the primitive equations: I. The basic
517 experiment. *Mon. Weather Rev.* **1963**, *91* (3), 99-164.
- 518 (39) Wu, H.; Tang, X.; Wang, Z.; Wu, L.; Lu, M.; Wei, L.; Zhu, J. Probabilistic Automatic
519 Outlier Detection for Surface Air Quality Measurements from the China National Environmental
520 Monitoring Network. *Adv. Atmos. Sci.* **2018**, *35* (12), 1522-1532.
- 521 (40) Liu, J.; Mauzerall, D. L.; Horowitz, L. W.; Ginoux, P.; Fiore, A. M. Evaluating inter-
522 continental transport of fine aerosols: (1) Methodology, global aerosol distribution and optical
523 depth. *Atmos. Environ.* **2009**, *43* (28), 4327-4338.
- 524 (41) Anenberg, S. C.; West, J. J.; Yu, H.; Chin, M.; Schulz, M.; Bergmann, D.; Bey, I.; Bian,
525 H.; Diehl, T.; Fiore, A.; Hess, P.; Marnmer, E.; Montanaro, V.; Park, R.; Shindell, D.; Takemura,

- 526 T.; Dentener, F. Impacts of intercontinental transport of anthropogenic fine particulate matter on
527 human mortality. *Air Qual. Atmos. Health* **2014**, 7 (3), 369-379.
- 528 (42) Chin, M.; Diehl, T.; Ginoux, P.; Malm, W. Intercontinental transport of pollution and dust
529 aerosols: implications for regional air quality. *Atmos. Chem. Phys.* **2007**, 7 (21), 5501-5517.
- 530 (43) Wang, J.; Zhang, M.; Bai, X.; Tan, H.; Li, S.; Liu, J.; Zhang, R.; Wolters, M. A.; Qin, X.;
531 Zhang, M.; Lin, H.; Li, Y.; Li, J.; Chen, L. Large-scale transport of PM_{2.5} in the lower
532 troposphere during winter cold surges in China. *Sci. Rep.* **2017**, 7, No. 13238.
- 533 (44) Yu, H.; Remer, L. A.; Chin, M.; Bian, H.; Tan, Q.; Yuan, T.; Zhang, Y. Aerosols from
534 overseas rival domestic emissions over North America. *Science* **2012**, 337 (6094), 566-569.

535

536 TOC Art



537

538

(For Table of Contents Only)

539